A parameter-free perfectly matched layer formulation for the finite-element-based solution of the Helmholtz equation

Radu Cimpeanu[a,*], Anton Martinsson[b], Matthias Heil[c]

[a]*Department of Mathematics, Imperial College London, SW7 2AZ, London, United Kingdom, Tel. No.:+44 (0)7723 541154, Fax.:+44 (0)161 275 5819, E-mail:radu.cimpeanu11@imperial.ac.uk*
[b]*School of Mathematics, University of Manchester, Oxford Road, Manchester M13 9PL, United Kingdom, Tel. No.:+44 (0)7557 375827 E-mail:anton.martinsson@student.manchester.ac.uk*
[c]*School of Mathematics, University of Manchester, Oxford Road, Manchester M13 9PL, United Kingdom, Tel. No.:+44 (0)161 275 5808, E-mail:matthias.heil@manchester.ac.uk*

Abstract

This paper presents a parameter-free perfectly matched layer (PML) method for the finite-element-based solution of the Helmholtz equation. We employ one of Bermúdez *et al.*'s unbounded absorbing functions for the complex coordinate mapping underlying the PML. With this choice, the only free parameter that controls the accuracy of the numerical solution for a fixed numerical cost (characterised by the number of elements in the bulk and the PML regions) is the thickness of the perfectly matched layer, $\delta_{\rm PML}$. We show that, for the case of planar waves, the absorbing function performs best for PMLs whose thickness is much smaller than the wavelength. We then perform extensive numerical experiments to explore its performance for non-planar waves, considering domain shapes with smooth and polygonal boundaries, different solution types (smooth and singular), and a wide range of wavenumbers, k, to identify an optimal range for the normalised PML thickness, $k\delta_{\rm PML}$, such that, within this range, the error introduced by the presence of the PML is consistently small and insensitive to change. This implies that if the PML thickness is chosen from within this range

*Corresponding author
URL: `http://www3.imperial.ac.uk/people/radu.cimpeanu11` (Radu Cimpeanu), `http://www.maths.manchester.ac.uk/~mheil/` (Matthias Heil)

no further PML optimisation is required, i.e. the method is parameter-free. We characterise the dependence of the error on the discretisation parameters and establish the conditions under which the convergence of the solution under mesh refinement is controlled exclusively by the discretisation of the bulk mesh.
Keywords: Perfectly matched layers, Helmholtz equation, acoustic scattering, finite element method.

---

1. Introduction

Many problems that involve the propagation of time-harmonic waves are naturally posed in unbounded domains. For instance, a common problem in the area of acoustic scattering is the determination of the sound field that is generated when an incoming time-harmonic wave (which is assumed to arrive "from infinity") impinges onto a solid body (the scatterer). The boundary conditions to be applied on the surface of the scatterer (typically of Dirichlet, Neumann or Robin type) tend to be easy to enforce in most numerical solution schemes. Conversely, the imposition of a suitable decay condition (typically a variant of the Sommerfeld radiation condition [1]), which is required to ensure the well-posedness of the solution, is considerably more involved. As a result, many numerical schemes generate spurious reflections from the outer boundary ∂D_c of the finite computational domain D_c.

Popular methods for the imposition of the radiation condition (and/or conditions that allow scattered waves to leave the computational domain without being reflected at its outer boundary) include local absorbing boundary conditions (ABCs). These can be derived either by formulating conditions that aim to minimise the reflection of waves from ∂D_c [2], or by matching the numerical solution to the general solution of the relevant wave equation in the far field ([3]; [4]). ABCs are easy to implement within a finite-element-based solution scheme (see, e.g., [5]) and they retain the sparsity of the system matrix. However, they are only accurate if applied at large distances from the scatterer, thus requiring the use of large computational domains. This limitation can be reduced by the

use of high-order local non-reflecting ABCs [6].

An alternative approach is given by Dirichlet-to-Neumann (DtN) mappings which match the solution in the computational domain to a far field solution via an integral equation that is defined on the outer boundary of the computational domain (see, e.g., [7, 8, 9]). DtN-based boundary conditions can be applied close to the scatterer but create a direct coupling between the degrees of freedom on the boundary of the computational domain, resulting in a dense sub-block in the system matrix which makes the solution of the associated linear system costly. We refer to [10] for a more detailed discussion of these methods.

In the present paper we will concentrate on the imposition of the radiation condition by perfectly matched layers (PMLs) which were first introduced by Bérenger [11] in the context of electromagnetic wave propagation. PML methods employ a complex coordinate transformation which turns propagating waves into damped waves when they enter a layer of elements that surrounds the computational domain. They combine the advantages of both previous methods since they are easy to implement, retain the sparsity of the system matrix, and can be applied close to the boundary of the scatterer. The methodology has since been extended to other wave equations and is now widely used for the numerical solution of problems in acoustic scattering [12, 13], seismology [14, 15], linear elasticity [16, 17, 18], and ultrasound [19], to name but a few.

All three methods discussed above introduce errors into the numerical solution and contain parameters that control the magnitude of that error. For PML-based methods the error is controlled by the functional form of the complex coordinate mapping (the absorbing function), the thickness of the layer that surrounds the computational domain, and the number of elements used to discretise it. Unfortunately, the optimisation of these parameters in order to obtain the best numerical solution for a given computational effort is non-trivial and often highly problem-dependent [18, 20, 21, 22, 23, 24]. Recently, Bermúdez *et al.* [25] proposed a novel unbounded absorbing function which ensures that (in the continuous setting) spurious reflections off the boundary of the computational domain are completely suppressed for planar waves governed by the 2D

Helmholtz equation. Numerical experiments for a variety of 2D acoustic scattering problems demonstrated that the method works extremely well (and much better than many previously used absorbing functions) for problems involving non-planar waves too. Rabinovich *et al.* [26] subsequently also showed that the method outperforms the commonly used polynomial absorbing functions and presents significant advantages over ABC-based discretisations. A key feature of Bermúdez *et al.*'s approach is that the only parameter to be adjusted in order to achieve the optimal numerical solution for a given computational effort is the thickness of the PML region.

In the present paper we analyse the dependence of the error on this quantity. We show the existence of an optimal range of (normalised) PML thicknesses for which the error of the numerical solution is small and insensitive to change. This implies that, as long as the PML thickness is chosen from within that range, its specific value has no effect on the result and is therefore not a parameter that needs to be optimised. Thus we arrive at a parameter-free optimal PML method for the finite-element-based solution of the 2D Helmholtz equation.

The structure of the paper is as follows. We start with a brief review of the finite-element-based discretisation of the 2D Helmholtz equation and give details of Bermúdez *et al.*'s [25] absorbing function. In section 3 we first show analytically that, for the case of planar waves, the absorbing function performs best for PMLs whose thickness is much smaller than the wavelength. We then report the results of extensive numerical experiments on three test problems. These reveal the existence of an optimal range of (normalised) PML thicknesses for which the error of the numerical solution is small and insensitive to changes in that thickness. We show that, for a sufficiently large number of elements in the PML region, the error is completely controlled by the bulk discretisation and decreases at the optimal theoretical convergence rate. For non-planar waves, the presence of the PML ultimately leads to a saturation of the error under further bulk mesh refinement. We analyse the dependence of the error on the bulk and PML discretisation and demonstrate in section 3.3 that the optimal convergence rate under bulk mesh refinement can be maintained if the number of element

layers in the PML is increased in proportion to the number of elements per wavelength in the bulk. Finally, we summarise our results and discuss possible extensions in section 4.

2. Problem setup

We consider the solution of the 2D Helmholtz equation

$$\nabla^2 u + k^2 u = 0 \tag{1}$$

for a real wavenumber k, in an infinite domain D with interior boundary $\partial D = \partial D_{\mathrm{D}} \cup \partial D_{\mathrm{N}}$, subject to Dirichlet boundary conditions on ∂D_{D},

$$u\big|_{\partial D_{\mathrm{D}}} = u_0, \tag{2}$$

Neumann boundary conditions on ∂D_{N},

$$\left.\frac{\partial u}{\partial n}\right|_{\partial D_{\mathrm{N}}} = g_0, \tag{3}$$

and the Sommerfeld radiation condition [1]

$$\lim_{r\to\infty} r^{1/2}\left(\frac{\partial u}{\partial r} - \mathrm{i}ku\right) = 0. \tag{4}$$

We wish to solve equations (1)-(4) in a finite (computational) domain of interest, D_{c}, using a finite element method, and applying the Sommerfeld radiation condition (4) by a perfectly matched layer technique. For this purpose we employ the usual complex coordinate mapping [27]

$$\frac{\partial}{\partial x_i} \to \frac{1}{\gamma_i(x_i)}\frac{\partial}{\partial x_i}, \tag{5}$$

and multiply (1) by $\gamma_1\gamma_2$, which transforms it into

$$\frac{\partial}{\partial x_1}\left(\frac{\gamma_2}{\gamma_1}\frac{\partial u}{\partial x_1}\right) + \frac{\partial}{\partial x_2}\left(\frac{\gamma_1}{\gamma_2}\frac{\partial u}{\partial x_2}\right) + k^2\gamma_1\gamma_2 u = 0. \tag{6}$$

We surround the domain of interest, D_{c}, by axis-aligned PML regions of constant width, δ_{PML}, and choose the complex functions γ_i as

$$\gamma_i = \begin{cases} 1 & \text{in } D_{\mathrm{c}} \\ 1 + \frac{\mathrm{i}}{k}\sigma_i(\nu_i) & \text{otherwise,} \end{cases} \tag{7}$$

where $\nu_i \in [0, \delta_{\mathrm{PML}}]$ is the normal distance of a point in the PML region from the boundary of D_{c} along which $x_i = const$; see Fig. 1. It is well known that the coordinate transformation described above ensures that, as long as the real-valued absorbing functions σ_i are positive, any propagating waves that enter the PML region (i) do so without being reflected at the interface ∂D_{c}, and (ii) are then rapidly attenuated within that region (see section 3.1 for details). Provided the PML region is sufficiently thick and/or σ_i sufficiently large, the propagating waves decay so rapidly that their reflections at the outer boundary of the PML region (where we apply the homogeneous Dirichlet boundary condition $u = 0$) are very weak; furthermore, the reflected waves are attenuated yet further while they return through the PML region to the domain of interest, leading to minimal artificial reflections from ∂D_{c} into D_{c}.

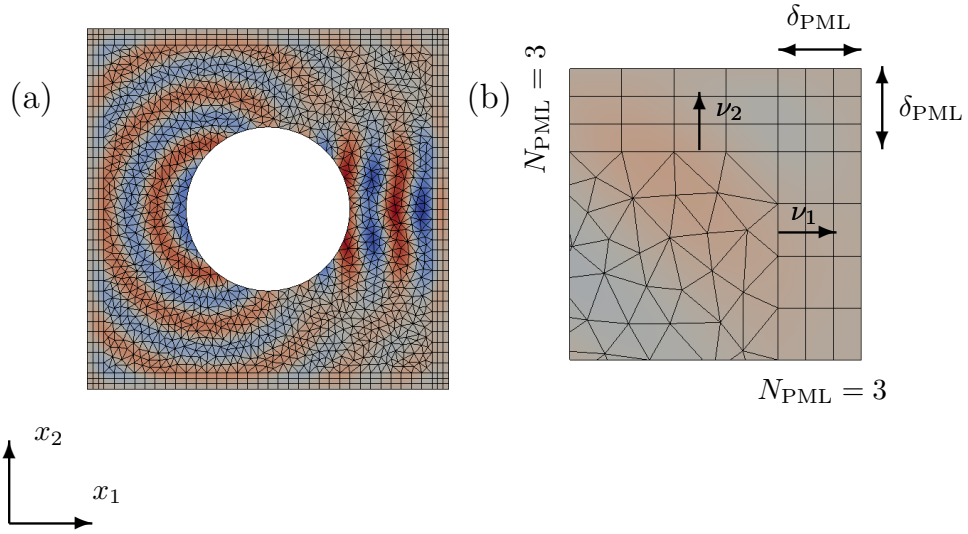

Figure 1: (a) Plot of a typical hybrid finite element mesh, comprising an unstructured mesh of triangular elements (the bulk mesh) for the discretisation of the domain of interest, D_c, surrounded by a layer of quadrilateral PML elements. (b) Detail of the top right corner of the mesh, illustrating the parameters that characterise the PML discretisation.

Unfortunately, none of these desirable features are completely preserved when the problem is discretised and, as usual, a trade-off then has to be found between computational cost and the accuracy of the numerical solution. PML methods therefore have to be optimised to achieve the best possible solution for a given computational cost. For a hybrid mesh comprising an unstructured mesh of triangular elements in D_{c} (which we will occasionally refer to as the bulk mesh) and a conforming structured mesh of quadrilaterals elements in the PML region, as shown in Fig. 1, the accuracy of the solution is controlled by:

1. The order p of the finite element basis functions (e.g. piecewise linear ($p = 1$), quadratic ($p = 2$) or cubic ($p = 3$)).
2. The typical element size in the region of interest, D_{c}, characterised, e.g. in terms of the number of elements per wavelength
$$\mathcal{N} = \frac{2\pi}{kh}, \tag{8}$$
where h is the typical edge length of the elements used to discretise D_{c}.
3. The number of element layers, N_{PML}, in the PML regions.
4. The thickness of the PML region, δ_{PML}.
5. The functional form of the absorbing functions σ_i.

Improvements via options 1-3 (i.e. via h- or p-refinement) increase the computational cost. PML optimisation at fixed cost has traditionally focused on tuning the absorbing functions σ_i, while keeping the thickness of the PML regions, δ_{PML}, fixed and typically comparable to the wavelength or some problem-specific lengthscale; see e.g. [22, 28]. Rabinovich *et al.* [26] analysed the effect of variations in δ_{PML} and N_{PML} on the accuracy of the solution, but restricted themselves to PML thicknesses within that range. Popular choices for σ_i are powers of the normal distance from ∂D_c, i.e. functions of the form $\sigma_i = S\nu_i^n$ which, for $S, n > 0$, gradually increase the strength of the attenuation into the PML region. Unfortunately, the optimal choice of the constants n and S is highly problem- and mesh-dependent; see, e.g., [20, 21, 24].

Recently, Bermúdez *et al.* [25] proposed an interesting alternative approach by considering absorbing functions that are singular at the outer boundary of

the PML region. Specifically, they showed that the choice

$$\sigma_i = \frac{1}{\delta_{\mathrm{PML}} - \nu_i}, \tag{9}$$

is optimal in the sense that (in the continuous setting) it completely suppresses the reflection of planar waves with arbitrary incidence angle off the boundary of the domain of interest. (Bermúdez *et al.*'s expression for the damping function, equation (5.2) in their paper, includes the wavespeed c, which can be set to 1 by a suitable non-dimensionalisation of the equations.)

They performed numerical experiments using piecewise linear ($p = 1$) elements to show that (9) systematically outperformed traditional polynomial absorbing functions. Possibly the most important property of Bermúdez *et al.*'s absorbing function is that the sole parameter to be optimised is the thickness of the PML region, δ_{PML}, which Bermúdez *et al.* kept constant in all their numerical experiments. We shall demonstrate below that variations in δ_{PML} (with all other parameters kept constant) can have a strong effect on the accuracy of the numerical solution and will then identify an optimal choice for δ_{PML}. Thus we propose a truly parameter-free PML method for the finite-element-based solution of the 2D Helmholtz equation.

3. Optimisation of the PML thickness δ_{PML}

3.1. The optimal PML thickness for the case of planar waves

To analyse how the performance of Bermúdez *et al.*'s damping function (9) depends on the PML thickness, δ_{PML}, we initially consider the case of a planar wave, propagating in the x_1-direction,

$$u = \exp(\mathrm{i}kx_1), \tag{10}$$

which we wish to resolve in a computational domain $D_{\mathrm{c}} = \{(x_1, x_2) \mid x_1 \in [0, 1]\}$, bounded by a PML region $D_{\mathrm{PML}} = \{(x_1, x_2) \mid x_1 \in [1, 1 + \delta_{\mathrm{PML}}]\}$. We now recall that the PML method is based on the complex coordinate transformation

$$\widehat{x_1}(x_1) = \begin{cases} x_1 & \text{for } x_1 \in [0, 1] \\ x_1 + \frac{\mathrm{i}}{k} \displaystyle\int_1^{x_1} \sigma(s)\, ds & \text{for } x_1 \in [1, 1 + \delta_{\mathrm{PML}}], \end{cases} \tag{11}$$

and that the application of this coordinate transformation to any exact solutions of the original Helmholtz equation (1), provides an exact solution of the modified Helmholtz equation (6) in the entire domain $D_c \cup D_{\mathrm{PML}}$. The exact solution for the 1D planar travelling wave problem is therefore given by

$$u = \exp(\mathrm{i}kx_1)\ f(x_1), \tag{12}$$

where

$$f(x_1) = \begin{cases} 1 & \text{for } x_1 \in [0,1] \\ \exp\left(-\displaystyle\int_1^{x_1} \sigma(s)\ ds \right) & \text{for } x_1 \in [1, 1+\delta_{\mathrm{PML}}]. \end{cases} \tag{13}$$

This shows that, as long as $\sigma(s) > 0$, the solution decays rapidly (exponentially for $\sigma(s) = const.$) inside the PML, and is therefore very small (but in general nonzero) at the outer edge of the PML region. The imposition of a zero Dirichlet boundary condition at the outer edge of the PML region is therefore (slightly) inconsistent with the exact solution and in general causes (very small) reflections. Our key observation is that Bermúdez *et al.*'s damping function (9) does not suffer from this problem. Inserting (9) into (13) yields

$$f(x_1) = \begin{cases} 1 & \text{for } x_1 \in [0,1] \\ \dfrac{1+\delta_{\mathrm{PML}} - x_1}{\delta_{\mathrm{PML}}} & \text{for } x_1 \in [1, 1+\delta_{\mathrm{PML}}], \end{cases} \tag{14}$$

implying that the exact solution is obtained by pre-multiplying the original solution (10) by a piecewise linear function that is exactly zero at the outer edge of the PML region and therefore consistent with the application of homogeneous Dirichlet boundary conditions. This provides an alternative interpretation of Bermúdez *et al.*'s observation (which they derived via the analysis of the reflection coefficient) that their damping function completely suppresses the reflection of planar waves.

Both Bermúdez *et al.*'s and our own analysis only apply in the continuous setting but our interpretation of their results allows insight into the discretisation required to represent this exact solution on a finite element mesh. For

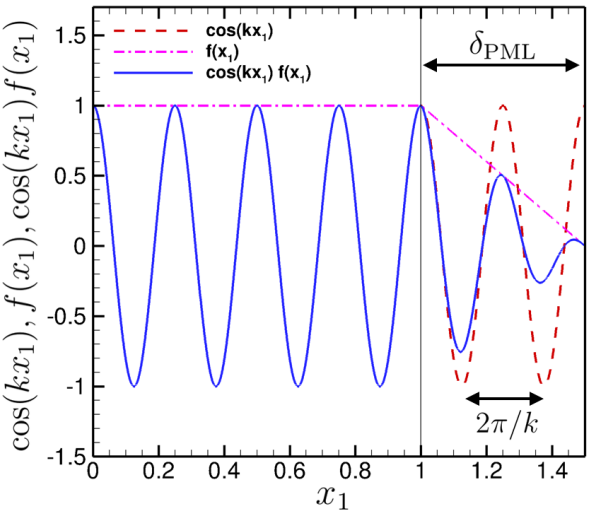

Figure 2: Plot of the real part of the 1D travelling solution, $\cos(kx_1)$ (dashed line) and its counterpart after the PML coordinate transformation, $Re(u) = \cos(kx_1)f(x_1)$ (solid line). The thin vertical line indicates the outer boundary of the computational domain.

this purpose we note that the plot of the real part of the solution, $Re(u) = \cos(kx_1)f(x_1)$, and its constituent factors in Fig. 2 shows that the number of elements in the PML region required to accurately represent this solution depends on the ratio of the PML thickness, $\delta_{\rm PML}$ to the wavelength $2\pi/k$, i.e. it is controlled by the value of the normalised PML thickness, $k\delta_{\rm PML}$. If $k\delta_{\rm PML} = \mathcal{O}(1)$, the exact solution oscillates within the PML region (as in Fig. 2) and can therefore only be resolved by a large number of finite elements. Conversely, as $k\delta_{\rm PML} \to 0$ the solution in the PML region approaches a straight line because $\cos(kx_1)$ remains virtually constant over the width of the PML region. The solution can therefore be approximated to high accuracy with even a single linear element inside the PML region. We note that the slope of the solution is discontinuous at the outer edge of the computational domain, ∂D_c. This does not cause any problems if the equations are discretised with Lagrange-type finite elements which allow for such discontinuities at element boundaries.

Our analysis suggests that Bermúdez *et al.*'s damping function will perform

best if the PML thickness is chosen such that $k\delta_{\rm PML} \ll 1$. However, we expect that in actual computations there will be a lower limit of $\delta_{\rm PML}$ beyond which the distortion of the elements in the PML region will cause numerical problems. Furthermore, the analysis presented so far only applies to planar waves. In the next section we will therefore present the results of comprehensive numerical experiments by which we explore these ideas for a number of increasingly challenging test cases.

3.2. Numerical Experiments

To assess the effect of variations in the PML thickness $\delta_{\rm PML}$ on the quality of actual numerical solutions we performed numerical experiments using a standard Galerkin discretisation of the transformed Helmholtz equation (6), employing Lagrange-type finite elements with linear, quadratic or cubic basis functions. The equations were implemented in `oomph-lib`, the open-source object-oriented multi-physics finite element library [29], freely available at `http://www.oomph-lib.org`. `SuperLU`, a sparse direct solver [30], was used to solve the linear systems.

In test cases where an exact solution, $u_{\rm ex}$, is available we characterised the accuracy of the numerical solution, $u_{\rm FE}$, in terms of the normalised L^2 error, computed over the domain of interest, $D_{\rm c}$, (excluding the PML regions),

$$\mathcal{E} = \left(\frac{\int_{D_{\rm c}} |u_{\rm FE} - u_{\rm ex}|^2 \; dx_1 \; dx_2}{\int_{D_{\rm c}} |u_{\rm ex}|^2 \; dx_1 \; dx_2} \right)^{1/2} . \tag{15}$$

The integration is always carried out on the mesh on which the actual computation is performed, using the same elemental Gauss integration scheme that is used to evaluate the finite element matrices and vectors. In cases where an analytical solution is known, we evaluated $u_{\rm ex}$ directly at the relevant Gauss points. In cases where no exact solution is available and the reference solution was pre-computed on a finer mesh, we evaluated the equivalent of $u_{\rm ex}$ on the finer mesh via its own finite element interpolant.

3.2.1. Test case 1: A one-dimensional waveguide

We start with the simple, quasi-one-dimensional test case discussed in section 3.1 and solve the Helmholtz equation in the rectangular domain $D_\mathrm{c} = \{(x_1, x_2) \mid x_1 \in [0,1];\ x_2 \in [0,H]\}$. The application of the Dirichlet boundary condition $u = 1$ at the left boundary (at $x_1 = 0$), and homogeneous Neumann boundary conditions $\partial u/\partial n = \pm\partial u/\partial x_2 = 0$ at the top and bottom boundaries (at $x_2 = 0$ and $x_2 = H$, respectively) makes the 1D travelling wave solution (10) the exact solution of this problem.

Since the solution is independent of x_2 we discretise D_c using a single row of (square) quadrilateral elements of constant edge length h and set the (arbitrary) height of the domain to $H = h$. We then aim to suppress reflections off the right boundary (at $x_1 = 1$) with a PML region of width δ_PML, which we discretise with another N_PML (rectangular) quadrilateral elements. We apply homogeneous Neumann boundary conditions at their top and bottom boundaries, and the homogeneous Dirichlet condition $u = 0$ at $x_1 = 1 + \delta_\mathrm{PML}$. With this setup it is possible to perform computations with very large numbers of elements per wavelength since the total number of unknowns in the problem increases linearly with $\mathcal{N}$.

Fig. 3 shows the dependence of the error, $\mathcal{E}$, on the normalised PML thickness, $k\delta_\mathrm{PML}$, for a range of wavenumbers ($k = 8, 16, 32$ and 64) and different numbers of elements in the PML region ($N_\mathrm{PML} = 1, 2, 4, 8$ and 16, distinguished by the different symbols). For all computations shown in this figure, we used piecewise quadratic basis functions ($p = 2$), and set the number of elements per wavelength in D_c to $\mathcal{N} = 100$ to ensure that $\mathcal{E}$ is dominated by the error due to the PML.

The figure shows a very robust behaviour that is consistent with the analysis presented in section 3.1. Since N_PML is kept constant along the various curves, an increase in δ_PML makes it more and more difficult to resolve the solution in the PML region. A rise in $k\delta_\mathrm{PML}$ beyond $\approx 10^{-2}$ therefore leads to a rapid increase in $\mathcal{E}$. The error can be reduced by an increase in N_PML though this

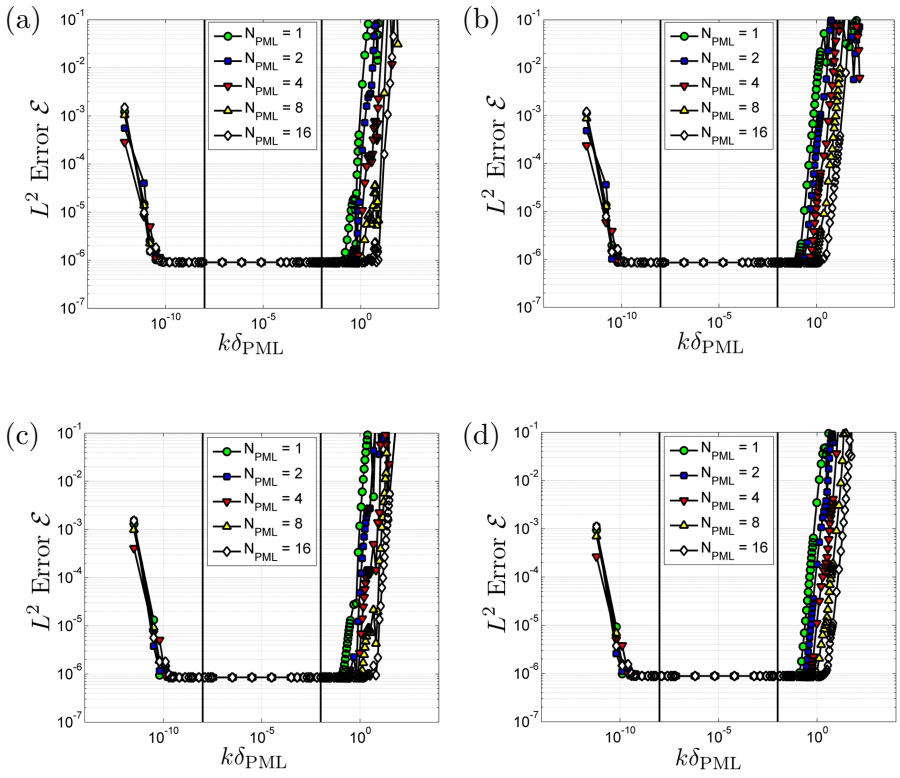

Figure 3: Error $\mathcal{E}$ as a function of the normalised PML thickness, $k\delta_{\mathrm{PML}}$, and the number of element layers in the PML region, N_{PML}, for Test Case 1. (a) $k = 8$, (b) $k = 16$, (c) $k = 32$, (d) $k = 64$. All computations were performed with $\mathcal{N} = 100$ elements per wavelength in the bulk, and with quadratic basis functions, $p = 2$. The vertical lines delimit the optimal parameter regime $\mathbb{I}_{\mathrm{opt}}$ within which the error is small and insensitive to changes in the thickness of the PML region.

obviously incurs additional computational cost.

For smaller values of the PML thickness, the solution in the PML region is sufficiently close to a linear function of x_1 that it is easy to resolve with a very small number of elements. As a result, in this regime the error obtained for $N_{\rm PML} = 1$ is practically identical to that obtained with a much finer spatial resolution (e.g. $N_{\rm PML} = 16$). This is illustrated further in Fig. 4 where we plot the exact (solid lines) and computed (dashed lines) solutions for $k = 8$ for three different values of the PML thickness. All computational results in this figure were obtained with linear elements ($p = 1$) and a fine bulk discretisation ($\mathcal{N} = 100$) to ensure that the error is dominated by the presence of the PML region which we discretised with a single element, $N_{\rm PML} = 1$. The left column shows the overall solution; in the right column we plot the solutions near the boundary of the computational domain as a function of the normalised coordinate $\nu_1/\delta_{\rm PML}$, where $\nu_1 = x_1 - 1$ is the distance from the outer edge of the computational domain. This normalisation ensures that the PML region is always located between 0 and 1 and facilitates the comparison between the solutions for different PML thicknesses. The oscillations of the exact solution in the PML region for $\delta_{\rm PML} = 1.0$ (shown in the top row of the figure) can clearly not be resolved by this discretisation and the error in the overall solution is therefore very large. A reduction in $\delta_{\rm PML}$ reduces the number of waves that are contained in the PML region and this greatly improves the accuracy of the computed solution. For $\delta_{\rm PML} = 10^{-6}$ (in the bottom row of the figure), the exact and computed solutions become graphically indistinguishable.

Returning now to Fig. 3, we observe that for even smaller PML thicknesses, $k\delta_{\rm PML} < 10^{-8}$, when the elements in the PML region become rather distorted, the error $\mathcal{E}$ increases again. We performed numerical experiments to show that the rise in the error in this regime is correlated with the rapidly increasing inaccuracy of the numerical integration scheme. In all our computations the elements' contributions to the matrix and right hand side of the global linear system that determines the solution were computed with "full integration", using standard Gauss rules of sufficient accuracy to evaluate products of any two

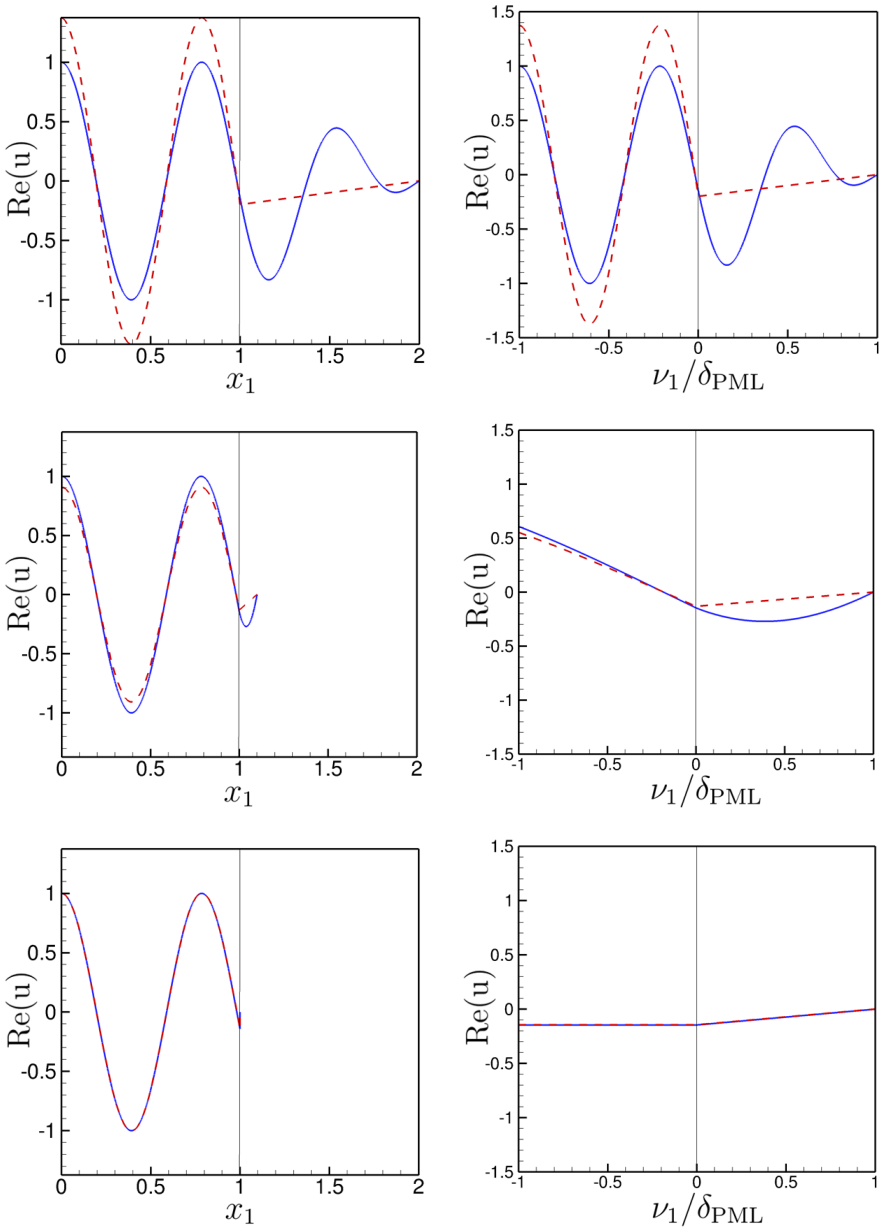

Figure 4: The exact (solid lines) and computed (dashed lines) solutions for Test Case 1 for various PML thicknesses [$\delta_{\mathrm{PML}} = 1.0$ (top), 0.1 (middle) and 10^{-6} (bottom)], plotted over the entire computational domain, $x_1 \in [0, 1 + \delta_{\mathrm{PML}}]$ (left) and near the boundary of the computational domain $x_1 \in [1 - \delta_{\mathrm{PML}}, 1 + \delta_{\mathrm{PML}}]$ (right). The thin vertical line indicates the outer boundary of the computational domain. All computations are for $k = 8$ and were performed with linear elements ($p = 1$) and $\mathcal{N} = 100$, $N_{\mathrm{PML}} = 1$.

basis functions exactly (this requires the use of $(p+1) \times (p+1)$-node tensor-product Gauss rules for quadrilateral elements with basis functions of order p; see, e.g., [31]). We compared the entries in the numerically computed elemental matrices against their exact counterparts, obtained by evaluating the relevant integrals using `maple`. As expected, the elemental matrices associated with elements in the bulk (for which the integrands are low-order polynomials in x_1) were found to be accurate to machine precision, while those associated with elements in the PML region generally contained small errors because the presence of the singular absorbing functions (9) in the transformed Helmholtz equation (6) turned the integrands into rational functions. Interestingly, the error introduced by the numerical integration only became significant in a regime when even the evaluation of the exact integrals in `maple` became numerically difficult and required the computations to be performed with 200 digits, indicating that in this regime roundoff errors are beginning to have an increasingly detrimental effect on the accuracy of the computation.

We note that for very small values of $\delta_{\rm PML}$ the bulk and PML meshes contain elements of extremely different sizes. This has the potential to cause ill-conditioning of the finite element matrix which may limit the accuracy of the solution of the linear system by the direct solver. We investigated this possibility by monitoring the condition number of the finite element matrices which we found to display only a very modest increase with a reduction in $\delta_{\rm PML}$. The assumption that this increase is insignificant is confirmed by the fact that `oomph-lib` actually treats all problems as nonlinear and solves the discretised equations by Newton's method. For linear problems with well-conditioned finite element matrices this method converges in one iteration. Based on our experience with other problems, ill-conditioning of the finite element matrix tends to result in additional Newton iterations or even cause the convergence of the Newton method to stall. None of this behaviour was observed in any of the computations we performed. Ill-conditioning of the finite element matrix is therefore unlikely to be responsible for the increase in the error at small PML thicknesses.

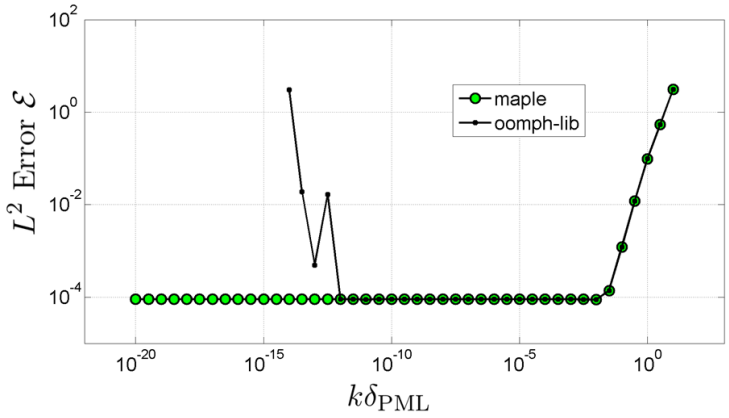

Figure 5: Error $\mathcal{E}$ as a function of the normalised PML thickness, for Test Case 1 with $k = 8$, discretised with $\mathcal{N} = 250$ linear elements per wavelength in the bulk and a single element in the PML, $N_{\rm PML} = 1$. The small markers show the error obtained when using our finite element code `oomph-lib`. The larger markers represent the error obtained when the entire finite-element computation is performed in `maple`, using an accuracy of 200 digits when evaluating symbolic expressions numerically.

This explanation for the rise of the error at extremely small values of $k\delta_{\rm PML}$ is further supported by Fig. 5, which shows a plot of the error as a function of the normalised PML thickness, $k\delta_{\rm PML}$, for the same discretisation as in Fig. 4 (linear elements, a single element in the PML region but $\mathcal{N} = 250$ elements per wavelength in the bulk). The small markers show the error when solving the equations with our finite element code, within which the integrals are evaluated numerically and all computations are performed in double precision arithmetic. The larger markers show the error obtained when re-implementing the entire finite element computation in `maple`, evaluating all integrals analytically and performing the final floating point evaluation of the results with an accuracy of 200 digits. Over most of the range of PML thicknesses both formulations give exactly the same result, but the `maple` computation does not display the rise in the error for extremely small values of $k\delta_{\rm PML}$. In fact, it is possible to analytically perform the limit $k\delta_{\rm PML} \to 0$ within `maple`. The result obtained for this case is identical to that obtained for the final (finite) value of the PML thickness

shown in this plot. While performing these computations we also monitored the condition number of the `maple`-generated finite-element matrix. We found that it also tended to a constant as $k\delta_{\rm PML}$ was reduced. The limiting value agreed with the condition number of the finite-element matrix obtained by actually setting $\delta_{\rm PML} = 0$. This proves that the rise in the error for small values of the PML thickness observed in Fig. 3 is due to the use of numerical integration in the evaluation of the finite-element matrices, and the finite precision arithmetic employed in the code. We note that, since the elements in the PML region are right-angled quadrilaterals, the contributions to the finite-element matrix and the right hand side of the linear system could, in principle, be computed analytically, thus bypassing the error due to the numerical integration. Appendix A in [25] lists the relevant integrals for the case of linear elements.

The key feature that emerges from the results presented in Fig. 3 is the existence of a large intermediate range of PML layer thicknesses,

$$\mathbb{I}_{\rm opt} = \{k\delta_{\rm PML} \mid 10^{-8} < k\delta_{\rm PML} < 10^{-2}\}, \tag{16}$$

within which the error remains approximately constant and close to its overall minimum, virtually independent of $N_{\rm PML}$. This parameter regime is characterised by the fact that within it the PML thickness is so small that the solution in the PML region is close to linear (and therefore easy to represent on a finite element mesh) but not so small that the numerical integration of the finite element matrices becomes difficult.

Fig. 6 shows that the features observed in Fig. 3 (for $\mathcal{N} = 100$ and piecewise quadratic basis functions) are independent of the type of basis functions, and are not affected by variations in the bulk discretisation in the sense that for all values of $\mathcal{N}$ in the range $5 \leq \mathcal{N} \leq 100$, the error is small and insensitive to changes in the normalised PML layer thickness if $k\delta_{\rm PML} \in \mathbb{I}_{\rm opt}$. In all cases the error increases rapidly once the thickness of the PML layer exceeds $k\delta_{\rm PML} > 10^{-2}$. Conversely, the increase in $\mathcal{E}$ for very small PML thicknesses only arises once the bulk discretisation is sufficiently fine so that the error drops below $\mathcal{O}(10^{-4})$.

This indicates that, at least for the simple initial problem considered here,

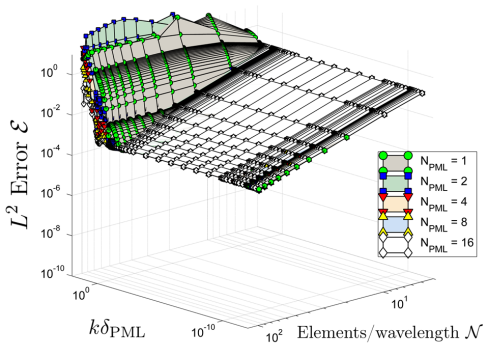

(a) $k = 8$, linear elements ($p = 1$)

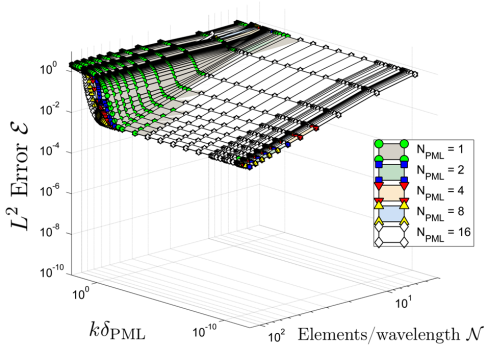

(b) $k = 64$, linear elements ($p = 1$)

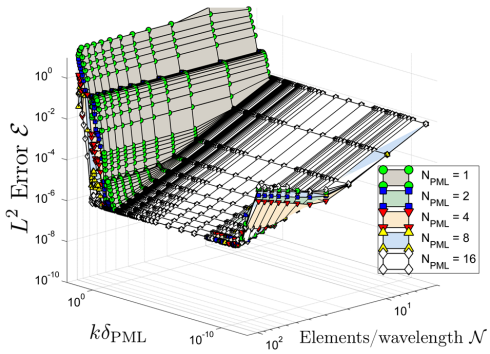

(c) $k = 8$, quadratic elements ($p = 2$)

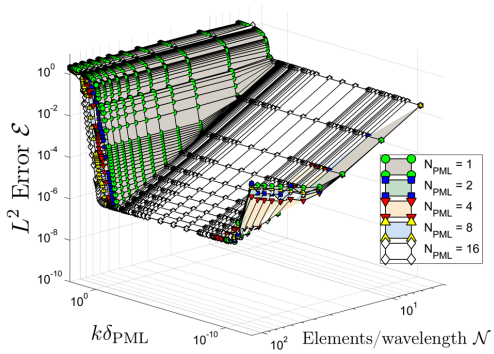

(d) $k = 64$, quadratic elements ($p = 2$)

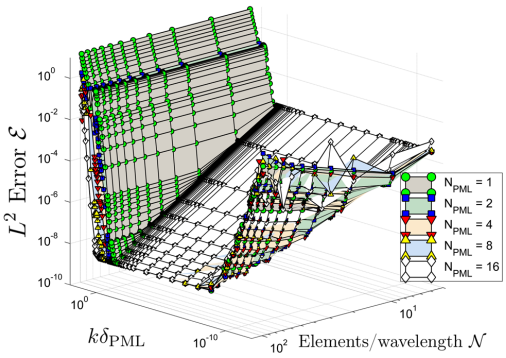

(e) $k = 8$, cubic elements ($p = 3$)

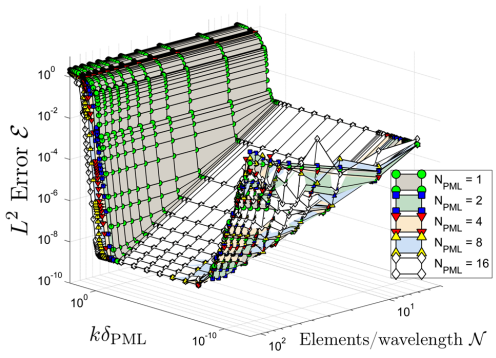

(f) $k = 64$, cubic elements ($p = 3$)

Figure 6: Error $\mathcal{E}$ as a function of the normalised PML thickness, $k\delta_{\mathrm{PML}}$, the number of elements per wavelength in the bulk, $\mathcal{N}$, and the number of element layers in the PML region, N_{PML}, for Test Case 1.

Bermúdez *et al.*'s absorbing function (9) yields optimal results for a given computational cost if it is applied with a normalised PML layer thickness from the optimal range $\mathbb{I}_{\text{opt}}$. In fact, Fig. 7 demonstrates that for the specific choice $\delta_{\text{PML}} = 10^{-6}$, so that $k\delta_{\text{PML}} \in \mathbb{I}_{\text{opt}}$ (and a single element in the PML region, $N_{\text{PML}} = 1$) the L^2 error behaves like $\mathcal{E} \sim \mathcal{N}^{-(p+1)}$ (for $p = 1, 2$ and 3) as $\mathcal{N}$ is increased, indicating that the error is completely controlled by the discretisation of the bulk mesh. We refer to [32, 33, 34] for a discussion of the optimal convergence rate of numerical solutions obtained from finite element discretisations of the Helmholtz equation and note that the observed convergence rate indicates that the bulk discretisation was always sufficiently fine to avoid dispersion errors.

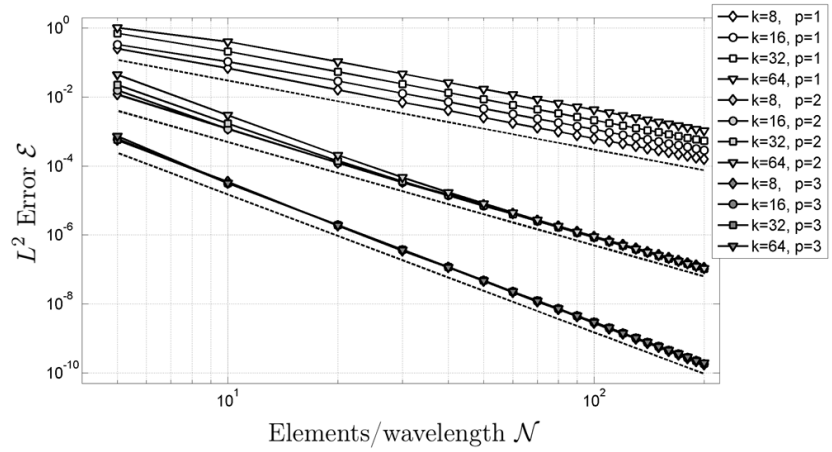

Figure 7: Error $\mathcal{E}$ for Test Case 1 as a function of the number of elements per wavelength in the bulk, $\mathcal{N}$, for various wavenumbers ($k = 8, 16, 32, 64$) and element types ($p = 1, 2, 3$). The PML discretisation is held fixed at $\delta_{\text{PML}} = 10^{-6}$ and $N_{\text{PML}} = 1$. The dashed lines indicate the optimal convergence rates under bulk mesh refinement $\mathcal{E} \sim \mathcal{N}^{-(p+1)}$.

3.2.2. Test case 2: Scattering of a planar wave off a cylinder

Guided by the insight obtained from the study of the simple quasi-one-dimensional model in the previous section, we now explore the approach in a genuinely two-dimensional scattering problem for which the general solution of

equation (1) representing outward propagating waves is given by

$$u(r,\theta) = \sum_{n=-\infty}^{\infty} A_n \; H_n^{(1)}(kr) \exp(\mathrm{i}n\theta), \tag{17}$$

where (r,θ) are cylindrical polar coordinates. The A_n are constant coefficients which are determined by the boundary conditions. For the numerical experiments presented below we chose

$$A_n = -\frac{\mathrm{i}^n J_n(k)}{H_n^{(1)'}(k)}. \tag{18}$$

With this choice, the solution (17) represents the scattered field generated by a planar sound wave, propagating in the x_1-direction, interacting with an impenetrable (sound-hard) cylinder of unit radius, centred at the origin of the coordinate system [35]; see Fig. 1 for a contour plot of this solution, which we obtained in a computational domain bounded by the lines $x_1 = \pm 2$ and $x_2 = \pm 2$.

Fig. 8 shows the variation of the error with $k\delta_{\mathrm{PML}}$, as in Fig. 3, again for a discretisation with piecewise quadratic basis functions, $p = 2$. (The range of wavenumbers considered here is smaller because the computational cost of the numerical simulations performed to obtain these results is significantly greater than in the quasi-one-dimensional case; the simulations with $k = 12$ involved up to 1.7 million unknowns.) We note that many features of Fig. 3 are observed here too. Specifically, for $k\delta_{\mathrm{PML}} < 10^{-8}$, the error increases with a reduction in the PML thickness. For larger values of the PML thickness the error is again virtually independent of $k\delta_{\mathrm{PML}}$, until beyond $k\delta_{\mathrm{PML}} = 10^{-2}$ the error begins to vary strongly with the thickness of the PML region. Careful adjustment of δ_{PML} in the regime where $k\delta_{\mathrm{PML}} = \mathcal{O}(1)$ (the range in which most previous attempts at PML optimisation have been performed) allows a reduction of the error by another order of magnitude. However, the precise value for which this optimum is achieved depends sensitively on N_{PML} and small changes to δ_{PML} from its global optimum can lead to a large increase in the error. Ultimately, the error increases significantly when the number of elements in the increasingly wide

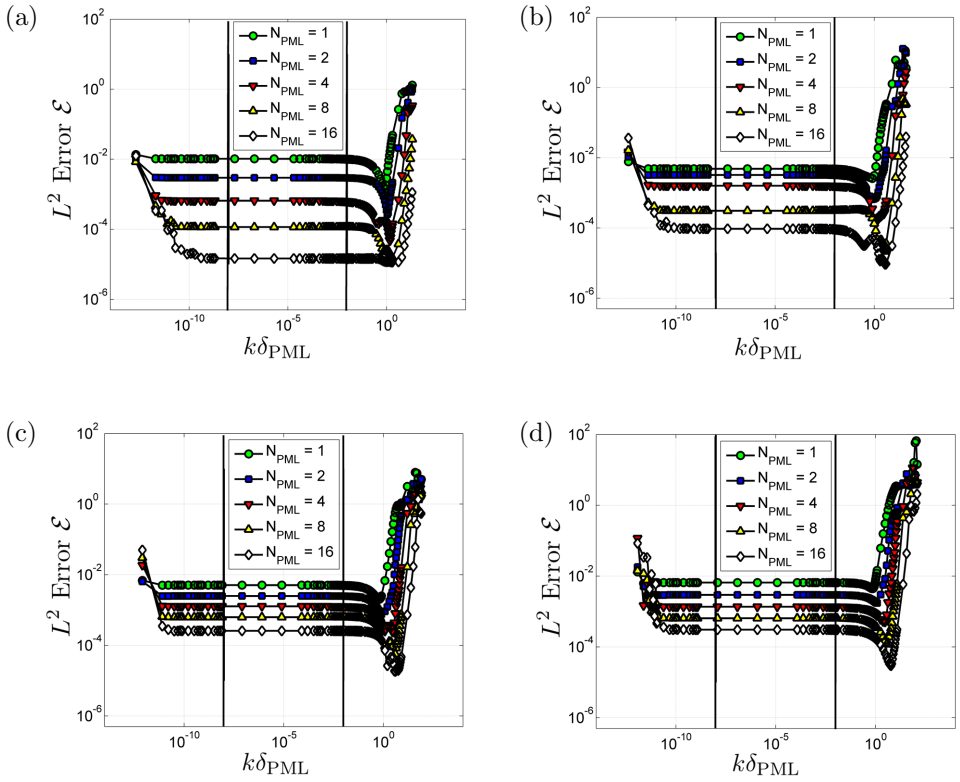

Figure 8: Error $\mathcal{E}$ as a function of the normalised PML thickness, $k\delta_{\mathrm{PML}}$, and the number of element layers in the PML region, N_{PML}, for Test Case 2. (a) $k = 2$, (b) $k = 4$, (c) $k = 8$, (d) $k = 12$. All computations were performed with $\mathcal{N} = 50$ elements per wavelength in the bulk and quadratic basis functions, $p = 2$. The vertical lines delimit the optimal parameter regime $\mathbb{I}_{\mathrm{opt}}$ within which the error is small and insensitive to changes in the thickness of the PML region.

PML region becomes insufficient to resolve the spatial variations of the solution in this region.

An important difference to the results shown in Fig. 3 is that if $k\delta_{\mathrm{PML}}$ is chosen from the optimal range the error displays a marked dependence on the number of element layers in the PML region, with an increase in N_{PML} consistently reducing the error (at additional computational cost). To explain this observation, Fig. 9 shows how the error depends on the bulk discretisation (characterised again by the number of elements per wavelength, $\mathcal{N}$, which we

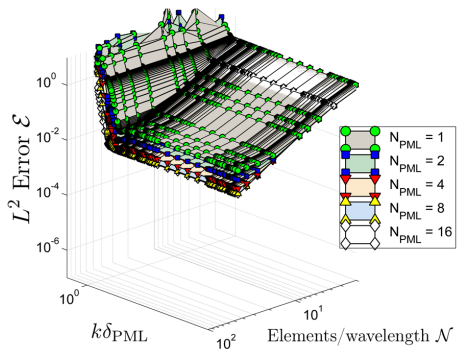

(a) $k = 4$, linear elements ($p = 1$)

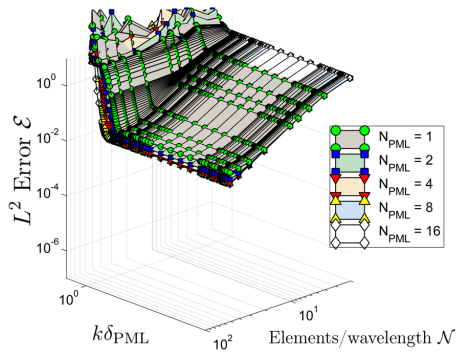

(b) $k = 12$, linear elements ($p = 1$)

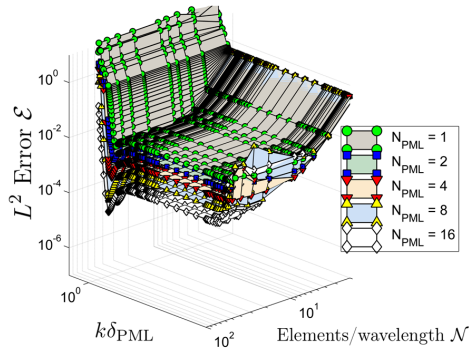

(c) $k = 4$, quadratic elements ($p = 2$)

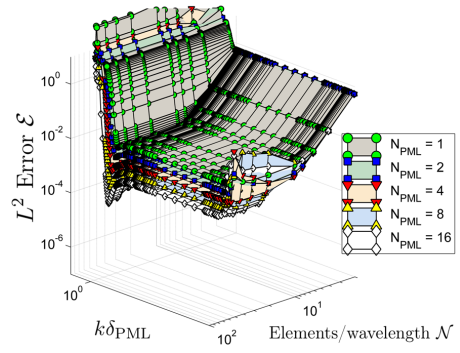

(d) $k = 12$, quadratic elements ($p = 2$)

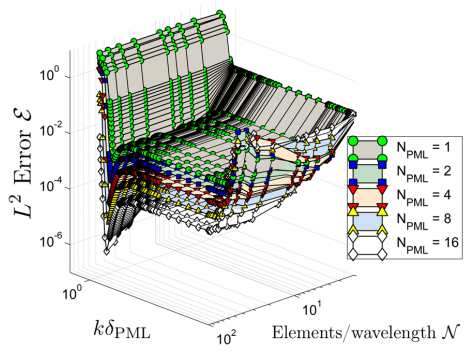

(e) $k = 4$, cubic elements ($p = 3$)

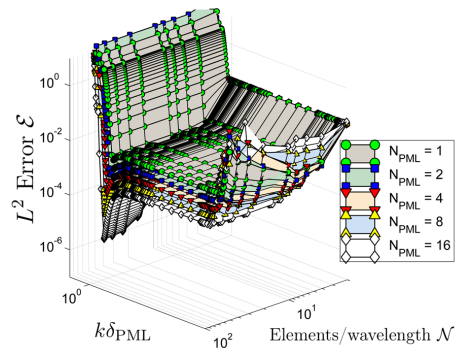

(f) $k = 12$, cubic elements ($p = 3$)

Figure 9: Error $\mathcal{E}$ as a function of the normalised PML thickness, $k\delta_{\mathrm{PML}}$, the number of elements per wavelength in the bulk, $\mathcal{N}$, and the number of element layers in the PML region, N_{PML}, for Test Case 2.

vary between 2 and 50). Overall, the figure is very similar to its counterpart for the quasi-one-dimensional case (Fig. 6). For a given discretisation of the PML region (i.e. for fixed $N_{\rm PML}$ and $k\delta_{\rm PML} \in \mathbb{I}_{\rm opt}$) an increase in the bulk resolution (via an increase in $\mathcal{N}$) initially reduces the error at the optimal rate $\mathcal{E} \sim \mathcal{N}^{-(p+1)}$ (see also Fig. 10), with little dependence on $N_{\rm PML}$ and $k\delta_{\rm PML}$, exactly as in Fig. 6). However, once the bulk discretisation has become sufficiently fine, the overall error saturates and becomes dominated by the error due to the discretisation of the PML region. The onset of the saturation can be delayed (and hence the reduction in the error with an increase in $\mathcal{N}$ continued to larger values of $\mathcal{N}$) by increasing $N_{\rm PML}$ (at additional computational cost).

The saturation of the error under bulk mesh refinement is illustrated more clearly by the plots in Fig. 10, which show the variation of the error with an increase in $\mathcal{N}$ for $\delta_{\rm PML} = 10^{-6}$, such that $k\delta_{\rm PML} \in \mathbb{I}_{\rm opt}$, for various wavenumbers ($k = 4, 8, 12$), basis functions ($p = 1, 2, 3$) and values of $N_{\rm PML}$. We note that the dependence of the error displayed in Fig. 10 on $\mathcal{N}$ and $N_{\rm PML}$ is well described by a relation of the form

$$\mathcal{E}(\mathcal{N}, N_{\rm PML}) = C\mathcal{N}^{-(p+1)} + \mathcal{E}_{\rm PML}(N_{\rm PML}) \tag{19}$$

where C is a constant that depends only weakly on k, and $\mathcal{E}_{\rm PML}(N_{\rm PML})$ defines the minimum error achievable with a given number of element layers in the PML region. $\mathcal{E}_{\rm PML}(N_{\rm PML})$ decreases approximately linearly with an increase in $N_{\rm PML}$. It is interesting to note that the saturation of the error under increasing bulk mesh refinement is not present in the corresponding results for Test Case 1, confirming, yet again, that Bermúdez *et al.*'s attenuation function is perfect (so that there is zero reflection from the PML layer into the bulk, at least in the continuous setting) only for planar waves.

3.2.3. Test case 3: Scattering off multiple polygonal scatterers

Finally, we assess the performance of our approach in a multiple-scattering problem in which an incoming planar wave, travelling in the negative x_1-direction, impinges on the boundary, $\partial D_{\mathbf{N}}$, formed by the polygonal `oomph-lib` logo, on

Linear elements ($p = 1$)

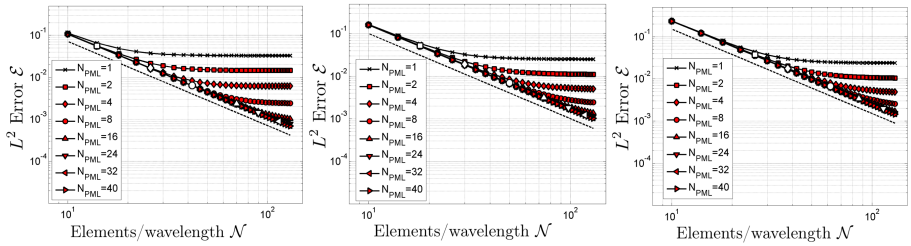

(a) $k = 4$ (b) $k = 8$ (c) $k = 12$

Quadratic elements ($p = 2$)

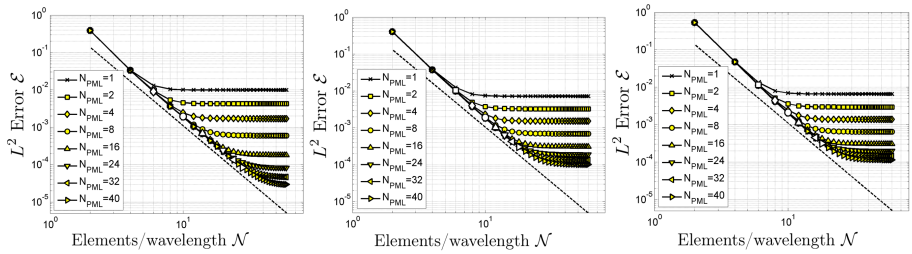

(d) $k = 4$ (e) $k = 8$ (f) $k = 12$

Cubic elements ($p = 3$)

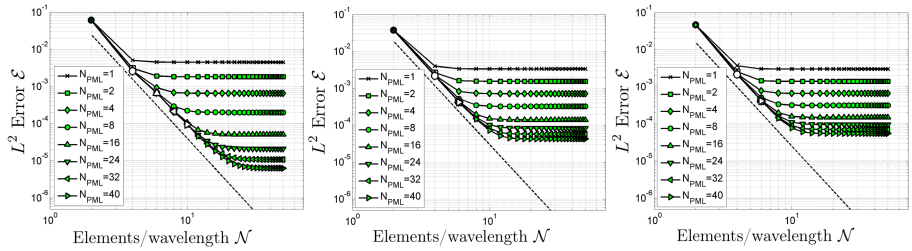

(g) $k = 4$ (h) $k = 8$ (i) $k = 12$

Figure 10: Error $\mathcal{E}$ for Test Case 2 as a function of the number of elements per wavelength in the bulk, $\mathcal{N}$, for various wavenumbers ($k = 4, 8, 12$) and element types ($p = 1, 2, 3$). The PML discretisation is held fixed at $\delta_{\text{PML}} = 10^{-6}$. The dashed lines indicate the optimal convergence rates under bulk mesh refinement, $\mathcal{E} \sim \mathcal{N}^{-(p+1)}$. The white symbols indicate the point at which the error is deemed to start saturating, based on the criteria used in section 3.3.

which we apply the Neumann boundary condition

$$\frac{\partial u}{\partial n} = \mathrm{i}kn_1 \exp(-\mathrm{i}kx_1), \tag{20}$$

where $\mathbf{n} = (n_1, n_2)$ is the outer unit normal on $\partial D_{\mathbf{N}}$. Fig. 11 shows the real part of the scattered field for $k = 40$, computed on a very coarse mesh with a thick PML region. A key feature of this problem is that the sharp re-entrant corners on the surface of the scatterer create a derivative singularity in the solution which limits the asymptotic convergence rate of the numerical solution under mesh refinement. Since there is no exact solution for this problem, we use the numerical solution computed with $\mathcal{N} = 180$, a PML layer thickness of $\delta_{\mathrm{PML}} = 10^{-6}$ and $N_{\mathrm{PML}} = 16$ as a proxy for u_{ex}. This involved the most expensive simulations performed in this study and required in excess of 10 million degrees of freedom for the most refined simulations with cubic elements.

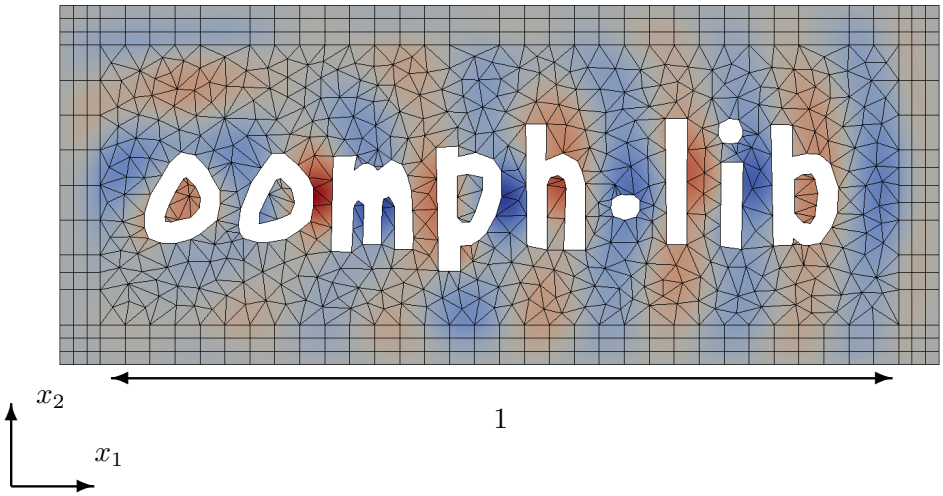

Figure 11: Plot of the solution of Test Case 3 for a wavenumber of $k = 40$ computed on a very coarse finite element mesh surrounded by a (relatively thick) PML.

Fig. 12(a) demonstrates that choosing δ_{PML} in the interval $\mathbb{I}_{\mathrm{opt}}$ identified

by the vertical lines in Fig. 12(a) again leads to a minimal error for fixed values of the discretisation parameters $\mathcal{N}$ and N_{PML} (here kept fixed at $\mathcal{N} = 22$ and $N_{\mathrm{PML}} = 16$) for linear, quadratic and cubic basis functions. Furthermore, Fig. 12(b) shows that for the specific choice $\delta_{\mathrm{PML}} = 10^{-6}$, such that $k\delta_{\mathrm{PML}} \in \mathbb{I}_{\mathrm{opt}}$, the error decays at the same rate $\mathcal{E} \sim \mathcal{N}^{-5/3}$ (shown by the dashed line) for all types of basis functions. This is consistent with the theoretically expected behaviour for domains with sharp re-entrant corners; see e.g. [36] for a discussion in the context of the Poisson equation.

We note that unlike the behaviour shown in Fig. 10, the error in Fig. 12(b) does not display any saturation under bulk mesh refinement, despite the fact that the scattered waves impinging on the PML boundary are non-planar. This is due to the fact that the error displayed in Fig. 12(b) was computed by referring to a numerical solution that was computed on a finer bulk mesh (larger $\mathcal{N}$) but with the same number of element layers in the PML region (same N_{PML}). Assuming that the actual error (relative to the (unknown) exact solution) in both numerical solutions has the functional form (19), the saturation error $\mathcal{E}_{\mathrm{PML}}$ is expected to cancel out. The absence of the saturation in Fig. 12(b) therefore provides further support for our conjecture that the actual error associated with Bermúdez *et al.*'s PML depends on the discretisation parameters $\mathcal{N}, N_{\mathrm{PML}}$ and p as described by equation (19). We have performed additional computations to confirm that the saturation error re-appears if the reference solution is computed with a larger number of elements in the PML region.

3.3. The saturation of the error for non-planar waves

The numerical results presented so far indicate that for a fixed computational effort (i.e. constant p, $\mathcal{N}$ and N_{PML}) there exists a range of normalised PML thicknesses such that for $k\delta_{\mathrm{PML}} \in \mathbb{I}_{\mathrm{opt}}$, the error remains small and typically close to the global minimum achievable. If the thickness of the PML region is chosen from within this range, the error may be reduced further by p-refinement, i.e. an increase in the order of the elements' basis functions; the benefit of h-refinement is generally limited because the presence of the PML causes the error

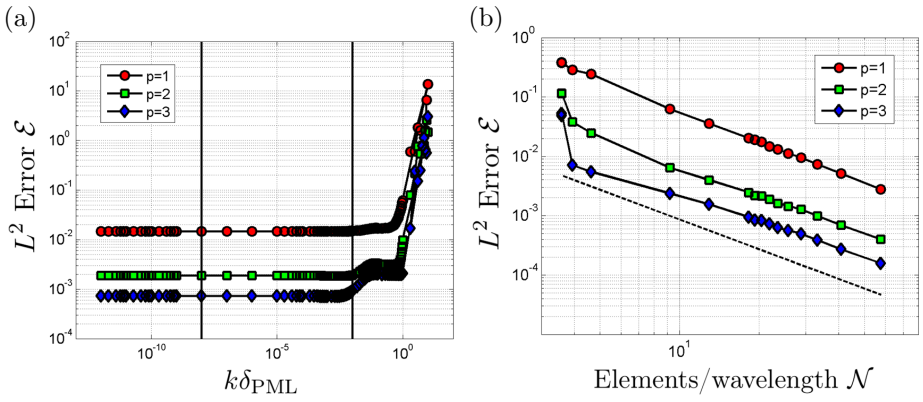

Figure 12: Results for Test Case 3 with $k = 40$. (a) Error $\mathcal{E}$ as a function of the normalised PML thickness, $k\delta_{\mathrm{PML}}$ for $\mathcal{N} = 22$ and $N_{\mathrm{PML}} = 16$. The vertical lines delimit the optimal parameter regime $\mathbb{I}_{\mathrm{opt}}$ defined in equation (16). (b) Error $\mathcal{E}$ as a function of the number of elements per wavelength in the bulk, $\mathcal{N}$, for three elements types ($p = 1, 2, 3$). The PML discretisation is held fixed at $\delta_{\mathrm{PML}} = 10^{-6}$ and $N_{\mathrm{PML}} = 16$. The dashed line indicates the optimal convergence rate under bulk mesh refinement, $\mathcal{E} \sim \mathcal{N}^{-5/3}$.

to saturate with increasing $\mathcal{N}$ (unless the solution consists of planar waves for which Bermúdez *et al.*'s [25] PMLs cause practically no reflection).

Since the onset of the saturation can be delayed by an increase in N_{PML} (see also [21, 23]), it is desirable to determine the minimum number of element layers in the PML region, $N_{\mathrm{PML}}^{\mathrm{min}}$, that is required to ensure that the quality of the numerical solution is controlled exclusively by the bulk discretisation so that for sufficiently smooth solutions the dependence of the error on the parameters $\mathcal{N}$ and p follows the asymptotic behaviour $\mathcal{E} \sim \mathcal{N}^{-(p+1)}$. To determine the dependence of $N_{\mathrm{PML}}^{\mathrm{min}}$ on $\mathcal{N}$ based on this criterion we note that in the log-log plots in Fig. 10 the curves representing the error for fixed N_{PML} contain two approximately straight segments – one in the region where the error decays according to the asymptotic error estimate, the other where the error has saturated and remains constant. To determine the transition between these two regimes (and thus the onset of the saturation) we fitted a spline to each of these curves and then determined the value $\widehat{\mathcal{N}}$ at which the slope of the spline associated with a

particular value of N_{PML} first deviated from the theoretical convergence rate by more than 10%. The pairs $(\widehat{\mathcal{N}}, N_{\mathrm{PML}})$ obtained by this procedure are shown by the white symbols in Fig. 10. They define the value N_{PML} required to (approximately) retain the theoretical convergence rate under bulk mesh refinement up to the spatial resolution associated with $\widehat{\mathcal{N}}$ and thus define $N_{\mathrm{PML}}^{\mathrm{min}}(\mathcal{N})$.

Fig. 13 indicates how $N_{\mathrm{PML}}^{\mathrm{min}}$ varies with $\mathcal{N}$ for the data from Test Case 2. The range over which data is displayed in Fig. 13 is determined by the range of $\mathcal{N}$ over which saturation is observed in Fig. 10. For linear elements ($p = 1$), $\widehat{\mathcal{N}}$ approaches the maximum value of $\mathcal{N}$ considered ($\mathcal{N} \leq 120$), while for the higher-order elements ($p = 2, 3$) saturation is observed at more modest values of $\mathcal{N}$ so that the original data is limited by the maximum number of element layers in the PML region ($N_{\mathrm{PML}} \leq 40$). Additional computations with up to $N_{\mathrm{PML}} = 240$ were therefore performed to extend the range of data available. Fig. 13 shows that in all cases the number of element layers in the PML region must increase linearly with the number of elements per wavelength in the bulk to retain the asymptotic convergence rate under (bulk) mesh refinement. While higher-order elements require much larger numbers of elements in the PML region to achieve this, it is important to stress that they tend to be much more accurate than their low-order counterparts and always give far more accurate results for given values of $\mathcal{N}$ and N_{PML}.

4. Summary and Conclusions

We have provided an alternative interpretation of Bermúdez *et al.*'s observation that, in a continuous setting, PMLs that are based on the unbounded damping function (9) do not cause any reflections for planar waves. This allowed us to show that, when discretised with conforming Lagrange-type finite elements, such PMLs perform best (for a given computational effort) when their thickness is chosen such that $k\delta_{PML} \ll 1$, i.e. if the thickness of the PML region is much smaller than the wavelength. Motivated by this observation we performed extensive numerical experiments to identify an optimal range of nor-

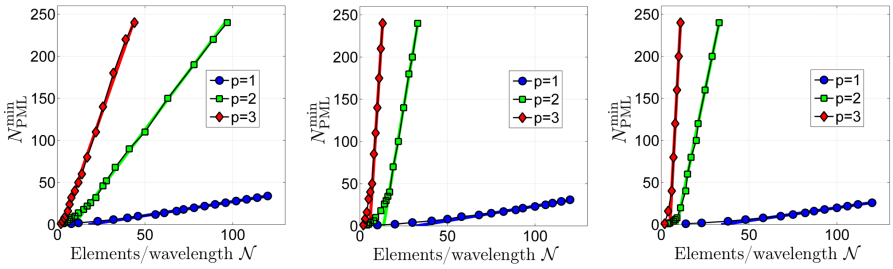

(a) k=4 (b) k=8 (c) k=12

Figure 13: The minimum number of element layers in the PML region, $N_{\mathrm{PML}}^{\mathrm{min}}$, required to maintain the optimal convergence rate under bulk mesh refinement for a) $k = 4$, b) $k = 8$ and c) $k = 12$ and the three element types ($p = 1, 2$ and 3) considered in this study. The thick solid lines are straight lines through the data points for large $\mathcal{N}$. PML thickness $\delta_{\mathrm{PML}} = 10^{-6}$ for all cases.

malised PML thicknesses, $\mathbb{I}_{\mathrm{opt}}$, such that for $k\delta_{\mathrm{PML}} \in \mathbb{I}_{\mathrm{opt}}$ Bermúdez *et al.*'s unbounded absorbing function (9) yields an error that is optimal (in the sense of being both small and insensitive to change) for a given computational cost (number of elements in the bulk and in the PML regions). Within the optimal parameter regime, the error remains small and virtually constant over several orders of magnitude of the normalised PML thickness $k\delta_{\mathrm{PML}}$. The optimal regime is bounded above by a regime in which the error increases due to insufficient spatial resolution in the PML region, and below by a regime in which the numerical integration becomes inaccurate. We stress that the optimal choice of the PML thickness does not require further optimisation within $\mathbb{I}_{\mathrm{opt}}$ since the error is virtually constant within this range. As long as $k\delta_{\mathrm{PML}}$ is chosen from within $\mathbb{I}_{\mathrm{opt}}$ its actual value is irrelevant since it neither affects the error nor the computational cost. Our recommendation to choose the normalised PML thickness $k\delta_{\mathrm{PML}}$ from anywhere within the optimal regime $\mathbb{I}_{\mathrm{opt}}$ therefore makes PML optimisation unnecessary and thus makes Bermúdez *et al.*'s PMLs parameter free.

Our simulations showed that for a sufficiently large number of element lay-

ers in the PML region, N_{PML}, the error is controlled exclusively by the bulk discretisation, which we characterised in terms of the number of elements per wavelength, $\mathcal{N}$. For a PML thickness from the optimal range, the error follows the theoretical error estimate ($\mathcal{E} \sim \mathcal{N}^{-(p+1)}$ for smooth solutions and $\mathcal{E} \sim \mathcal{N}^{-5/3}$ for solutions with derivative singularities) until the presence of the PML causes a saturation of the error under further bulk mesh refinement. The saturation in the error can be delayed by an increase in N_{PML} (at additional computational cost). We showed that a linear increase in N_{PML} together with an increase in $\mathcal{N}$ suffices to retain the theoretical convergence rate under bulk mesh refinement; see also [21, 23].

We note that Bermúdez *et al.* introduce a whole family of unbounded damping functions (types A-D, which all have a free parameter, β). They all share the property that, in the continuous setting, they completely suppress the reflection of planar waves with arbitrary incidence angle. In recent years other authors (e.g. [37, 38]) have also considered this class of functions and have conducted studies on the variation of the various parameters in their respective formulations (e.g. [26, 39]). It is therefore important to stress that the damping function (9) used in the present paper is *the only* function that has the key property that the complex coordinate mapping (11) transforms a planar travelling wave (10) into a linear function within the PML region as $k\delta_{\mathrm{PML}} \to 0$. It is interesting to note that Bermúdez *et al.* determined the optimal value of their parameter β via numerical experiments. These suggested $\beta = 1$ – precisely the value required to turn their type A function into (9). We refer to the Appendix for a more detailed discussion of Bermúdez *et al.*'s other unbounded damping functions.

As in Bermúdez *et al.*'s paper, our theoretical analysis applies only to the case of planar waves. We employed extensive numerical experiments to explore the optimal PML thickness in other settings. Given that these experiments included test cases with a variety of solution types (planar and non-planar waves; domains with smooth and polygonal boundaries; smooth and singular solutions; and a range of wavenumbers) and that we obtained consistent results for differ-

ent element types and an extremely wide range of spatial resolutions, we have confidence in the general nature of our results. Following the suggestion of a referee, we also explored the behaviour of Bermúdez *et al.*'s damping function with spectral elements (using nodal Legendre bases of various orders). The simulations (not presented here) showed the same behaviour that we reported for the low-order Lagrange-type finite elements. We suspect that our recommendation for the optimal thickness of the PML region also applies to the 3D Helmholtz equation, though the computational cost of performing equally comprehensive numerical experiments on 3D test problems would be considerable. It will be interesting to explore the performance of Bermúdez et al.'s absorbing functions in other wave equations, such as the equations of time-harmonic linear elasticity, to assess if our recommendation for the optimal thickness of the PML region applies here too. This work is currently in progress.

Acknowledgements

We would like to acknowledge the financial support of Thales UK Limited and the School of Mathematics at the University of Manchester. We are grateful to Phil Cotterill and Robert Harter for their comments on a draft of this manuscript. We also wish to thank the referees for their constructive comments and suggestions.

References

[1] A. Sommerfeld, Partial Differential Equations in Physics, Academic Press, New York, 1949.

[2] B. Engquist, A. Majda, Absorbing boundary conditions for the numerical simulation of waves, Mathematics of Computation 31 (139) (1977) 629–651.

[3] R. Mittra, O. Ramahi, Absorbing boundary conditions for the direct solution of partial differential equations arising in electromagnetic scattering

problems. PIER 2: Finite Element and Finite Difference Methods in Electromagnetic Scattering., M.A. Morgan, Elsevier, New York, 1990.

[4] A. Bayliss, M. Gunzburger, E. Turkel, Boundary conditions for the numerical solution of elliptic equations in exterior regions, SIAM Journal on Applied Mathematics 42 (1982) 430–451.

[5] J. Jin, The Finite Element Method in Electromagnetics, 2nd Edition, Wiley-Blackwell, New York, 2002.

[6] D. Givoli, High-order local non-reflecting boundary conditions: a review, Wave Motion 39 (2003) 319–326. doi:10.1016/j.wavemoti.2003.12.004.

[7] S.-K. Jeng, C.-H. Chen, On variational electromagnetics: theory and application, IEEE Transactions on Antennas and Propagation 32.

[8] R.-B. Wu, C. Chen, Variational reaction formulation of scattering problem for anisotropic dielectric cylinders, IEEE Transactions on Antennas and Propagation 34 (5) (1986) 640–645. doi:10.1109/TAP.1986.1143874.

[9] L. Pearson, R. Whitaker, L. Bahrmasel, An exact radiation boundary condition for the finite-element solution of electromagnetic scattering on an open domain, IEEE Transactions on Magnetics 25 (4) (1989) 3046–3048. doi:10.1109/20.34364.

[10] K. Ihlenburg, Finite Element Analysis of Acoustic Scattering, Springer-Verlag, New York, 1998.

[11] J.-P. Bérenger, A perfectly matched layer for the absorption of electromagnetic waves, Journal of Computational Physics 114 (2) (1994) 185 – 200. doi:http://dx.doi.org/10.1006/jcph.1994.1159.

[12] I. Harari, A survey of finite element methods for time-harmonic acoustics, Computer Methods in Applied Mechanics and Engineering 195 (1316) (2006) 1594 – 1607, a Tribute to Thomas J.R. Hughes on the Occasion of his 60th Birthday. doi:http://dx.doi.org/10.1016/j.cma.2005.05.030.

[13] X. Yuan, D. Borup, J. Wiskin, M. Berggren, R. Eidens, S. Johnson, Formulation and validation of Berenger's PML absorbing boundary for the FDTD simulation of acoustic scattering, IEEE Transactions on Ultrasonics, Ferroelectrics, and Frequency Control 44 (4) (1997) 816–822. doi:10.1109/58.655197.

[14] D. Komatitsch, R. Martin, An unsplit convolutional perfectly matched layer improved at grazing incidence for the seismic wave equation, Geophysics 72 (5) (2007) SM155–SM167. doi:10.1190/1.2939484.

[15] D. Komatitsch, J. Tromp, A perfectly matched layer absorbing boundary condition for the second-order seismic wave equation, Geophysical Journal International 154 (1) (2003) 146–153.

[16] U. Basu, A. Chopra, Perfectly matched layers for time-harmonic elastodynamics of unbounded domains: theory and finite-element implementation, Computer Methods in Applied Mechanics and Engineering 192 (2003) 1337–1375. doi:10.1016/S0045-7825(02)00642-4.

[17] G. Cohen, S. Fauqueux, Mixed spectral finite elements for the linear elasticity system in unbounded domains, SIAM Journal on Scientific Computing 26 (3) (2006) 864–884. doi:10.1137/S1064827502407457.

[18] K. Meza-Fajardo, A. Papageorgiou, A nonconvolutional, split-field, perfectly matched layer for wave propagation in isotropic and anisotropic elastic media: Stability analysis, Bulletin of the Seismological Society of America 98 (4) (2008) 1811–1836. doi:10.1785/0120070223.

[19] Y. Ukai, S. Ishida, N. Hata, T. Azuma, S. Umemura, T. Dohi, A $3-d$ simulation of focused ultrasound propagation for extracorporeal shock wave osteotomy, International Congress Series 1256 (1) (2003-06-01T00:00:00) 658–663. doi:10.1016/S0531-5131(03)00278-4.

[20] M. Kuzuoglu, R. Mittra, Investigation of nonplanar perfectly matched ab-

sorbers for finite-element mesh truncation, IEEE Transactions on Antennas and Propagation 45 (3) (1997) 474–486. doi:10.1109/8.558662.

[21] G. Pan, A. Abubakar, T. Habashy, An effective perfectly matched layer design for acoustic fourth-order frequency-domain finite-difference scheme, Geophysical Journal International 188 (1) (2012) 211–222. doi:10.1111/j.1365-246X.2011.05244.x.

[22] E. Bécache, A.-S. B.-B. Dhia, G. Legendre, Perfectly matched layers for the convected Helmholtz equation, in: G. C. Cohen, P. Joly, E. Heikkola, P. Neittaanmki (Eds.), Mathematical and Numerical Aspects of Wave Propagation WAVES 2003, Springer Berlin Heidelberg, 2003, pp. 142–147. doi:10.1007/978-3-642-55856-6-23.

[23] I. Singer, E. Turkel, A perfectly matched layer for the Helmholtz equation in a semi-infinite strip, Journal of Computational Physics 201 (2) (2004) 439–465. doi:10.1016/j.jcp.2004.06.010.

[24] X. Jiang, W. Zheng, Adaptive perfectly matched layer method for multiple scattering problems, Computer Methods in Applied Mechanics and Engineering 201204 (0) (2012) 42 – 52. doi:http://dx.doi.org/10.1016/j.cma.2011.09.013.

[25] A. Bermúdez, L. Hervella-Nieto, A. Prieto, R. Rodríguez, An optimal perfectly matched layer with unbounded absorbing function for time-harmonic acoustic scattering problems, Journal of Computational Physics 223 (2) (2007) 469 – 488. doi:http://dx.doi.org/10.1016/j.jcp.2006.09.018.

[26] D. Rabinovich, D. Givoli, E. Bécache, Comparison of high-order absorbing boundary conditions and perfectly matched layers in the frequency domain, International Journal for Numerical Methods in Biomedical Engineering 26 (10) (2010) 1351–1369. doi:10.1002/cnm.1394.

[27] F. Teixeira, W. Chew, A general approach to extend Berenger's absorbing boundary condition to anisotropic and dispersive media, IEEE

Transactions on Antennas and Propagation 46 (9) (1998) 1386–1387. doi:10.1109/8.719984.

[28] S. Kucukcoban, L. Kallivokas, A symmetric hybrid formulation for transient wave simulations in PML-truncated heterogeneous media, Wave Motion 50 (1) (2013) 57 – 79. doi:http://dx.doi.org/10.1016/j.wavemoti.2012.06.004.

[29] M. Heil, A. L. Hazel, `oomph-lib` – an object-oriented multi-physics finite-element library, in: M. Schäfer, H.-J. Bungartz (Eds.), Fluid-Structure Interaction, Springer, 2006, pp. 19–49, `oomph-lib` is available as open-source software at `http://www.oomph-lib.org`.

[30] J. W. Demmel, S. C. Eisenstat, J. R. Gilbert, X. S. Li, J. W. H. Liu, A supernodal approach to sparse partial pivoting, SIAM Journal on Matrix Analysis and Applications 20 (3) (1999) 720–755.

[31] K.-J. Bathe, Finite element procedures, 2nd Edition, Prentice-Hall, Englewood Cliffs, 1996.

[32] F. Ihlenburg, I. Babuška, Solution of Helmholtz problems by knowledge-based FEM, Computer Assisted Mechanics and Engineering Sciences 4 (1997) 397–415.

[33] I. Babuška, M. Suri, The p and h-p versions of the finite element method, basic principles and properties, SIAM Review 36 (1994) 4:578–632.

[34] I. Babuška, F. Ihlenburg, E. Paik, S. Sauter, A generalized finite element method for solving the Helmholtz equation in two dimensions with minimal pollution, Computer Methods in Applied Mechanics and Engineering 128 (1995) 325–359. doi:10.1016/0045-7825(95)00890-X.

[35] C. Linton, P. McIver, Handbook of mathematical techniques for wave/structure interactions, Chapman and Hall/CRC, London, 2001.

[36] H. Elman, D. Silvester, A. Wathen, Finite Elements and Fast Iterative Solvers, Oxford University Press, Oxford, 2005.

[37] J. Kormann, P. Cobo, A. Prieto, Perfectly matched layers for modelling seismic oceanography experiments, Journal of Sound and Vibration 317 (12) (2008) 354 – 365. doi:10.1016/j.jsv.2008.03.024.

[38] S. Ham, K.-J. Bathe, A finite element method enriched for wave propagation problems, Computers and Structures 9495 (0) (2012) 1 – 12. doi:10.1016/j.compstruc.2012.01.001.

[39] A. Modave, E. Delhez, C. Geuzaine, Optimizing perfectly matched layers in discrete contexts, International Journal for Numerical Methods in Engineering 99 (6) (2014) 410–437. doi:10.1002/nme.4690.

Appendix: The performance/behaviour of other unbounded damping functions

One of the key observations of our paper is that the damping function (9) is *the only* function that has the key property that the complex coordinate mapping (11) transforms a planar travelling wave (10) into a linear function within the PML region as $k\delta_{\mathrm{PML}} \to 0$. This observation explains why for sufficiently small values of the PML thickness even a single linear element suffices to represent the exact solution of the coordinate-transformed Helmholtz equation (6) within the PML region, implying that the accuracy of the overall solution is controlled exclusively by the bulk discretisation.

Bermúdez *et al.* [25] introduce a much wider class of unbounded damping functions which all have the property that, in the continuous setting, they yield zero reflection from the boundary of the computational domain. Our analysis suggests that their performance in a finite-element-based discretisation will depend crucially on how easy it is resolve this exact solution within the PML region on a finite-element mesh. Ignoring a possible multiplicative scaling factor

(which we discuss below), Bermúdez *et al.* [25] consider four different damping functions, Types A-D. All of these transform the travelling wave solution $u(x_1) = \exp(\mathrm{i}kx_1)$ into $f(x_1)\exp(\mathrm{i}kx_1)$, where $f = 1$ at the interface between the computational domain and the PML region, and $f = 0$ at the outer boundary of the PML region where we impose (consistent) homogeneous Dirichlet boundary conditions. The ease with which this exact solution can be represented on a finite-element mesh depends on the shape of $f(x_1)$ within the PML region.

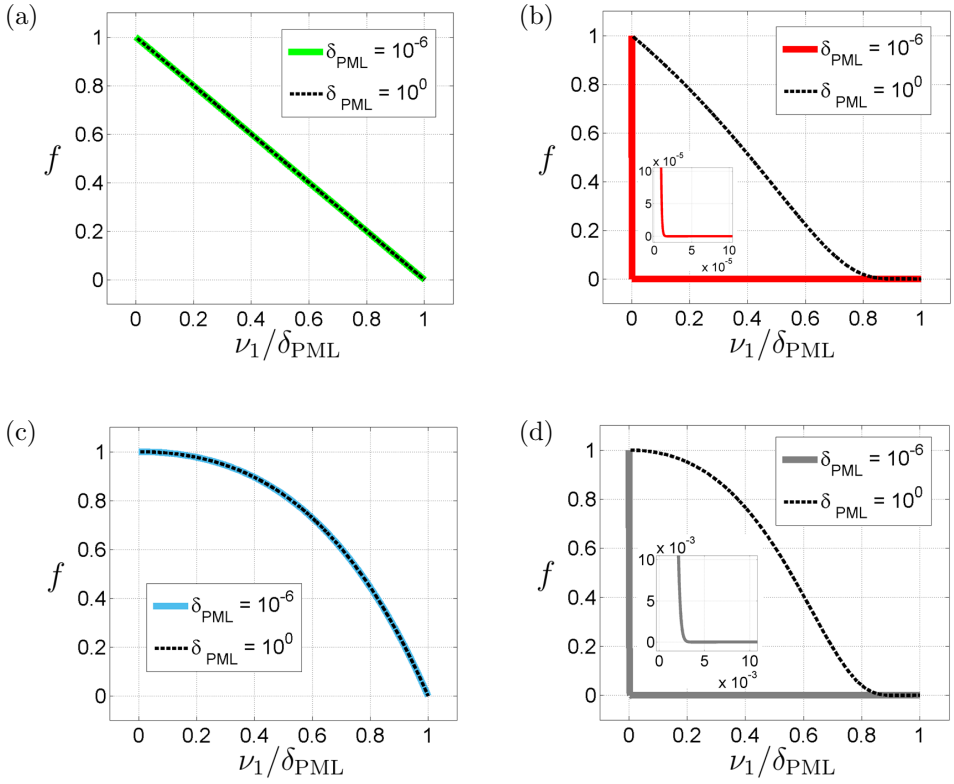

Figure 14: Prefactor f as a function of the normalised coordinate $\nu_1/\delta_{\mathrm{PML}}$, where $\nu_1 = x_1 - 1$ is the distance from the outer edge of the computational domain for (a) Type A, (b) Type B, (c) Type C and (d) Type D damping profiles. We present results for PML thicknesses $\delta_{\mathrm{PML}} = 10^0$ (dotted black lines) and $\delta_{\mathrm{PML}} = 10^{-6}$ (thick coloured lines). The inset in (b) and (d) shows a zoom into the region near the interface between the computational domain and the PML, to illustrate the extremely rapid variation of f for small PML thicknesses.

Type A:

$$\sigma(x_1) = \frac{1}{1 + \delta_{\mathrm{PML}} - x_1}.$$

This corresponds to our choice (9) and yields

$$f(x_1) = \frac{1 + \delta_{\mathrm{PML}} - x_1}{\delta_{\mathrm{PML}}},$$

a straight line across the PML, irrespective of the PML thickness. See Fig. 14(a).

Type B:

$$\sigma(x_1) = \frac{1}{(1 + \delta_{\mathrm{PML}} - x_1)^2}$$

This is obtained by raising the "Type A" function to the second power and thus leads to a more rapid attenuation of the solution within the PML. It yields

$$f(x_1) = \exp\left(\frac{1}{\delta_{\mathrm{PML}}} - \frac{1}{1 + \delta_{\mathrm{PML}} - x_1}\right).$$

Fig. 14(b) shows that this function is highly nonlinear and becomes increasingly steep near the interface between the computational domain and the PML region as $k\delta_{\mathrm{PML}} \to 0$, making it difficult to resolve on a finite element mesh. This function can therefore only be used for relatively large PML thicknesses, while using a sufficient number of elements in the PML to resolve the spatial variation to the required accuracy. The determination of the optimal values for N_{PML} and δ_{PML} requires a case-by-case numerical PML optimisation.

Type C:

$$\sigma(x_1) = \frac{1}{1 + \delta_{\mathrm{PML}} - x_1} - \frac{1}{\delta_{\mathrm{PML}}}.$$

This is obtained by the addition of the constant $1/\delta_{\mathrm{PML}}$ to the Type A function which makes $\sigma(x_1)$ continuous across the interface between the computational domain and the PML region. This may be advantageous in certain problems because it avoids the discontinuity in the slope of the solution at that interface. However, the presence of the constant distorts

the desirable linear variation of $f(x_1)$ within the PML region by an exponential,

$$f(x_1) = \frac{1 + \delta_{\text{PML}} - x_1}{\delta_{\text{PML}}} \exp\left(\frac{x_1 - 1}{\delta_{\text{PML}}}\right)$$

(see Fig. 14(c)), making it impossible to resolve the exact solution in the PML with a single linear element. The shape of the scaling factor is independent of δ_{PML}, therefore an increase in the number of elements in the PML region, N_{PML} (or an increase in the order of the finite element basis function, p) suffices to reduce the error, irrespective of the PML thickness.

Type D:

$$\sigma(x_1) = \frac{1}{(1 + \delta_{\text{PML}} - x_1)^2} - \frac{1}{\delta_{\text{PML}}^2},$$

is the continuous version of the Type B function. It corresponds to

$$f(x_1) = \exp\left(\frac{1}{\delta_{\text{PML}}} - \frac{1}{1 + \delta_{\text{PML}} - x_1} + \frac{x - 1}{\delta_{\text{PML}}^2}\right)$$

which suffers from the same problem as its discontinuous counterpart; see Fig. 14(d).

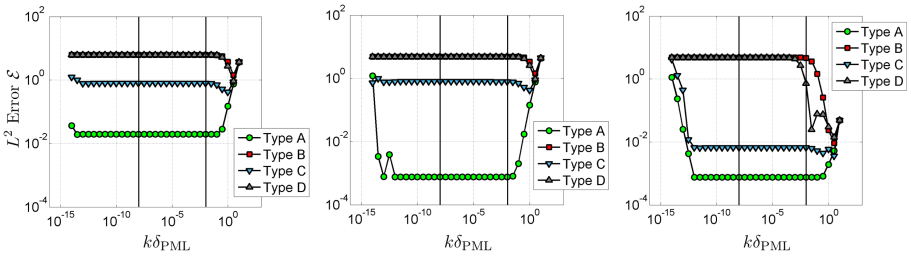

(a) $\mathcal{N} = 20, N_{\text{PML}} = 1$ (b) $\mathcal{N} = 100, N_{\text{PML}} = 1$ (c) $\mathcal{N} = 100, N_{\text{PML}} = 8$

Figure 15: Error $\mathcal{E}$ for Test Case 1 with $k = 8$ as a function of the normalised PML thickness, $k\delta_{\text{PML}}$ for damping profiles of Type A-D. (a) $\mathcal{N} = 20$ (b) $\mathcal{N} = 100$ linear elements per wavelength in the bulk, and a single element in the PML, $N_{\text{PML}} = 1$. (c) $\mathcal{N} = 100$ and $N_{\text{PML}} = 8$. The vertical lines delimit the parameter regime $\mathbb{I}_{\text{opt}}$ defined in equation (16).

Fig. 15 shows the dependence of the error on the normalised PML thickness for the quasi-one-dimensional Test Case 1 considered in section 3.2.1. The domain is discretised with (a) $\mathcal{N} = 20$ and (b,c) $\mathcal{N} = 100$ linear finite elements per wavelength in the bulk. In (a,b) the PML contains a single linear element, $N_{\mathrm{PML}} = 1$, while the results in (c) were obtained with $N_{\mathrm{PML}} = 8$. As expected, the Type B and D damping functions perform very poorly for thin PMLs. The error for the Type C function is much larger than that for the Type A function but for $k\delta_{\mathrm{PML}} \in \mathbb{I}_{\mathrm{opt}}$ the error remains approximately constant as δ_{PML} is reduced because the variation of $f(x_1)$ through the PML is independent of its thickness. The comparison between Figs. 15(a) and (b) shows that an increase in the bulk resolution (from $\mathcal{N} = 20$ to 100 elements per wavelength) only reduces the error for the Type A function. This is consistent with our assertion that the error associated with the Type C solution is controlled by the overly coarse discretisation of the PML – a single linear element cannot resolve a function that has the same shape as that shown in Fig. 14(c). Finally, Figs. 15(b) and (c) show the effect of an increase from $N_{\mathrm{PML}} = 1$ to 8 at a fixed bulk resolution ($\mathcal{N} = 100$). As expected, we find that for $k\delta_{\mathrm{PML}} \in \mathbb{I}_{\mathrm{opt}}$ the Type C solution benefits from this increase since it allows an improved resolution of the solution in the PML. Conversely, the error associated with the Type A solution remains unaffected since a single linear element is already sufficient to represent the profile shown in Fig. 14(a).

Having confirmed that, of the various damping functions considered by Bermúdez *et al.*, the Type A function performs best, we finally consider the effect of including a multiplicative constant B into the mapping function,

$$\sigma(x_1) = \frac{B}{1 + \delta_{\mathrm{PML}} - x_1}.$$

This yields the scaling factor

$$f(x_1) = \left(\frac{1 + \delta_{\mathrm{PML}} - x_1}{\delta_{\mathrm{PML}}} \right)^B.$$

The spatial variation of this function across the PML is independent of δ_{PML} but its shape depends crucially on the value of B. If $B = 1$ we recover (9);

for all other values the linear profile is distorted and thus unnecessarily difficult to resolve on a finite element mesh (with values in the range $B < 1$ being particularly problematic because of the infinite slope of $f(x_1)$ at the outer edge of the PML). We note that the constant B is the non-dimensional equivalent of Bermúdez *et al.*'s factor β which they determined by numerical experiments to yield optimal results if set to the wavespeed c – this corresponds precisely to $B = 1$.